Thermally Limited Current Carrying Ability of Graphene Nanoribbons

Albert D. Liao,[1,2] Justin Z. Wu,[3,4] Xinran Wang,[4] Kristof Tahy,[5] Debdeep Jena,[5] Hongjie Dai,[4,*] and Eric Pop[1,2,6,†]

[1]*Department of Electrical & Computer Engineering, University of Illinois at Urbana-Champaign, Urbana, Illinois 61801, USA*
[2]*Micro and Nanotechnology Lab, University of Illinois at Urbana-Champaign, Urbana, Illinois 61801, USA*
[3]*Department of Electrical Engineering, Stanford University, Stanford, California 94305, USA*
[4]*Department of Chemistry & Laboratory for Advanced Materials, Stanford University, Stanford, California 94305, USA*
[5]*Department of Electrical Engineering, University of Notre Dame, Notre Dame, Indiana 46556, USA*
[6]*Beckman Institute, University of Illinois at Urbana-Champaign, Urbana, Illinois 61801, USA*
(Received 25 January 2011; published 20 June 2011)

We investigate high-field transport in graphene nanoribbons (GNRs) on SiO_2, up to breakdown. The maximum current density is limited by self-heating, but can reach >3 mA/μm for GNRs ~15 nm wide. Comparison with larger, micron-sized graphene devices reveals that narrow GNRs benefit from 3D heat spreading into the SiO_2, which enables their higher current density. GNRs also benefit from lateral heat flow to the contacts in short devices (< ~0.3 μm), which allows extraction of a median GNR thermal conductivity (TC), ~80 W m^{-1}K^{-1} at 20 °C across our samples, dominated by phonons. The TC of GNRs is an order of magnitude lower than that of micron-sized graphene on SiO_2, suggesting strong roles of edge and defect scattering, and the importance of thermal dissipation in small GNR devices.

DOI: 10.1103/PhysRevLett.106.256801 PACS numbers: 85.35.−p, 65.80.Ck, 72.80.Vp, 73.63.−b

Graphene nanoribbons (GNRs) are promising materials for nanoelectronics [1,2]; however, many unknowns persist about their electrical and thermal properties. Among these, the maximum current density of GNRs is important both for fundamental and practical reasons: it is relevant to know what its limiting mechanisms are, to know how it compares with carbon nanotubes (CNTs), and to determine the types of loads that GNR transistors could drive within a circuit. By comparison, the current in single-wall CNTs is limited to tens of microamperes in diffusive transport due to self-heating and optical phonon scattering [3,4], although larger currents can be achieved in short quasiballistic samples [5], under ambipolar transport [6], or under avalanche conditions [7]. However, GNRs differ from CNTs in two key aspects: first, they have edges which can cause significant scattering, affecting both electrical and thermal transport [1,8]; second, they lie flat on the substrate, which increases their heat dissipation compared to CNTs [9,10] and can lead to lesser heat-limited current degradation.

Here, we study high-field transport in GNRs on SiO_2 up to breakdown, and uncover key roles of heat dissipation both along and perpendicular to the device. We measure current densities >3 mA/μm (> 4×10^8 A/cm^2) in ~15 nm narrow GNRs, limited by Joule self-heating. Comparing GNRs of varying sizes with "large" (micron-sized) graphene devices provides evidence of how physical properties vary as dimensions are being physically confined. For instance, three-dimensional (3D) heat spreading from GNRs into the SiO_2 enables higher current density than in large graphene devices. The high-field behavior and breakdown of GNRs is also sensitive to their thermal conductivity (TC), enabling an extraction of this key parameter.

GNR devices as shown in Fig. 1 were fabricated from solution-deposited GNRs [11], with more details given in the supplement [12]. For comparison, larger exfoliated graphene (XG) samples were also created, with dimensions defined by oxygen plasma patterning. Both types of samples were placed on SiO_2 (t_{ox} = 300 nm)/Si substrates, with Si also serving as the backgate (G). Source

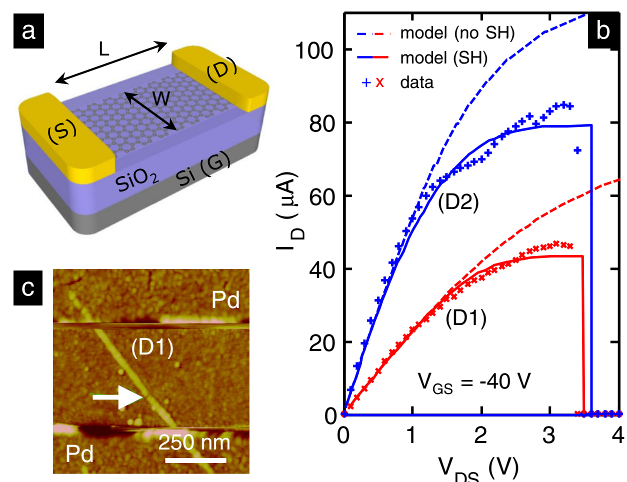

FIG. 1 (color online). (a) Schematic of graphene devices used in this work. (b) Measured (symbols) and simulated (lines) current vs voltage up to breakdown of GNRs in air. Solid lines are model with self-heating (SH) and breakdown when $\max(T) > T_{BD} = 873$ K, dashed lines are isothermal model without SH (see text and supplement [12]). Dimensions are $L/W = 510/20$ nm for D1, and $L/W = 390/38$ nm for D2. $V_{GS} = -40$ V to limit hysteresis effects. (c) Atomic force microscopy (AFM) image of D1 after high-current sweep; arrow shows breakdown location.

 © 2011 American Physical Society

(S) and drain (D) electrodes were made with Pd (20 nm) for GNRs and Cr/Au (2/200 nm) for XG devices. GNRs had widths ranging from $W = 15$–60 nm and lengths $L = 0.2$–0.7 μm. XG devices had $W = 0.1$–1.8 μm and lengths $L = 3.9$ and 9.7 μm.

To probe the limits of high-field transport, we measure $I_D - V_{DS}$ until devices break from Joule self-heating, as shown in Fig. 1(b). This is similar to the breakdown thermometry technique previously applied to CNTs [10,13] and nanowires [14]. Like with CNTs, the current drops sharply to zero, creating a small gap in the GNR as imaged in Fig. 1(c). Measurements were made in ambient air, where breakdown (BD) occurs by oxidation at $T_{BD} \approx 600\,^{\circ}$C [10]. By comparison, breakdown of control samples in vacuum ($\sim 7 \times 10^{-6}$ Torr) occurred at $\sim$6 times higher power (Fig. 2), suggesting other failure mechanisms such as defect formation, SiO_2 damage [10], or even GNR melting (graphite melts at $>$3600 °C, or $>$6 times the oxidation temperature [15]).

An existing graphene model [16,17] was adapted for GNRs [12], calculating I_D as a function of applied V_{GS}, V_{DS} and temperature T under diffusive transport conditions

$$I_D = qWV_{DS}\left[\int_0^L \frac{F_x}{n(V_{Gx}, T_x)\nu_d(F_x, T_x)}dx\right]^{-1}, \qquad (1)$$

where q is the elementary charge, x is the coordinate along the graphene channel, n is the total carrier density at location x, $V_{Gx} = V_G - V_x$ is the potential between gate and location x, $F_x = -dV_x/dx$ is the electric field, and ν_d is the drift velocity including saturation and temperature effects as in Ref. [17]. The current in Eq. (1) is solved self-consistently with the Poisson equation and the heat equation along the GNR [16], both including 3D fringing effects in the capacitance [12] and substrate heat dissipation [g in Eqs. (2) and (3) below]. Simulated $I_D - V_{DS}$ curves and breakdown voltages in Fig. 1(b) are in good agreement with the experimental data when self-heating (SH) is enabled in the model (solid lines). Without SH the simulated currents are much higher and breakdown cannot be modeled as the temperature remains unchanged.

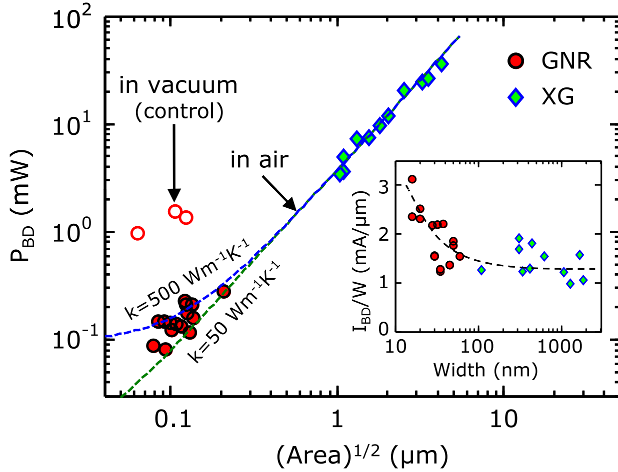

FIG. 2 (color online). Scaling of GNR and "large" XG breakdown power with square root of device footprint, $(WL)^{1/2}$. Dashed lines are thermal model with $k = 50$ and 500 W m^{-1}K^{-1}, $R_{Cox} = 5 \times 10^{-8}$ m^2 KW^{-1} and $L/W = 15$. Lateral heat sinking and in-plane GNR thermal conductivity begin to play a role in devices $< \sim 0.3$ μm (also see Fig. 3). A few GNRs were broken in vacuum as a control group (open circles). The inset shows scaling of peak current density vs width at T_{BD}, demonstrating greater current density in narrower GNRs that benefit from 3D heat spreading and lateral heat flow along the GNR. Dashed line drawn to guide the eye.

To gain more physical insight into the scaling of SH in such devices, we consider the power dissipated at breakdown, $P_{BD} = I_{BD}\,(V_{BD} - I_{BD}R_C)$ [10], where R_C is the electrical contact resistance [12], and I_{BD} and V_{BD} are the current and voltage at breakdown, respectively. We plot P_{BD} vs the square root of the device channel area in Fig. 2. To understand the scaling trend observed, we compare the experimental results with the analytic solution of the heat equation along the graphene devices, similar to CNTs [18]:

$$P_{BD} = gL(T_{BD} - T_0) \times \left[\frac{\cosh\left(\frac{L}{2L_H}\right) + gL_H R_T \sinh\left(\frac{L}{2L_H}\right)}{\cosh\left(\frac{L}{2L_H}\right) + gL_H R_T \sinh\left(\frac{L}{2L_H}\right) - 1}\right], \qquad (2)$$

where T_0 is the ambient temperature, L_H is the thermal healing length [18] along the graphene, and g is the thermal conductance to substrate per unit length [Eq. (3) below]. The thermal resistance at the metal contacts is $R_T \approx L_{Hm}/[k_m t_m(W + 2L_{Hm})]$. Here t_m is the thickness and $k_m \approx 22$ W m^{-1}K^{-1} is the TC of the metal electrodes (estimated with the Wiedemann-Franz law [19] using their measured resistivity), and L_{Hm} is the thermal healing length of heat spreading into the metal contacts. The two healing lengths are $L_H = (kWt/g)^{1/2}$ and $L_{Hm} = [k_m/(k_{ox}t_m t_{ox})]^{1/2}$, both of the order $\sim$0.1 μm here. The TC of SiO_2 $k_{ox} = 1.3$ W m^{-1}K^{-1}, while t is the thickness and k the TC of the graphene.

The heat loss coefficient into the substrate is different from CNTs and written as [12]

$$g^{-1} = \left\{\frac{\pi k_{ox}}{\ln[6(t_{ox}/W + 1)]} + \frac{k_{ox}}{t_{ox}}W\right\}^{-1} + \frac{R_{Cox}}{W}, \qquad (3)$$

which is the inverse of the series combination of the thermal resistance at the graphene/SiO_2 interface, R_{Cox} [20–22], and the 3D spreading thermal resistance into the SiO_2 written here as an analytic fit to detailed finite element simulations [12].

The two dashed lines in Fig. 2 show the predictions of the model for $k = 50$ and 500 W m^{-1}K^{-1}. We note that for device dimensions $(WL)^{1/2} \gg 0.3$ μm, or approximately 3 times the healing length L_H, heat dissipation is

essentially independent of heat flow along the graphene, and thus on its TC. As a result, dissipation in larger devices made with exfoliated graphene (XG) in Fig. 2 can also be estimated with the simplified approach in Ref. [17]. However, for GNRs with dimensions $\leq 3L_H$, heat dissipation occurs in part along the GNR, and this observation is used below to extract their TC. In the inset of Fig. 2 we plot the maximum current density I_{BD} per width W at breakdown (temperature $\sim T_{BD}$), and find it can reach over 3 mA/μm for the narrowest GNRs. This current density appears to scale inversely with width which, at first sight, is a counterintuitive finding compared to other (e.g., silicon) devices. This also appears at odds with the present understanding that GNRs have significantly lower mobility than large-area graphene [2,17].

We suggest that GNRs can dissipate more power and thus carry higher current density at a given temperature (here, breakdown temperature T_{BD}), consistent with a significant role of 3D heat spreading [9]. Figures 3(a) and 3(b) display the total device thermal conductance per unit area $G'' = P_{BD}/(T_{BD} - T_0)/(WL)$ obtained from the experiments (symbols) and the analytic model from Eq. (2) (solid lines). We note that for a given device the maximum power at breakdown, P_{BD} is proportional to G''. Similar to the inset of Fig. 2, we find that both the experimental data and our model scale inversely with the device width. In fact, while P_{BD} and G'' scale by a factor of ~ 9 over our data range (Fig. 3), I_{BD} scales by a factor of ~ 3 (Fig. 2 inset) as expected from Joule heating.

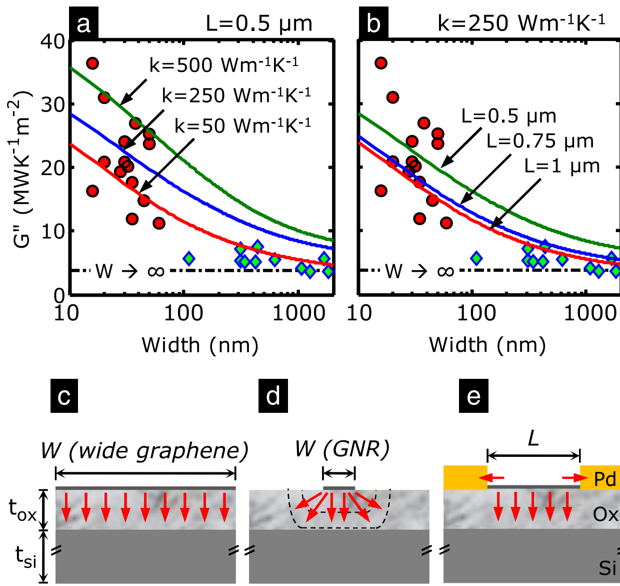

FIG. 3 (color online). Thermal conductance of device per unit area (G'') vs width for graphene of varying (a) thermal conductivity and (b) length. Both parameters affect heat sinking along GNRs $< \sim 0.3$ μm. Symbols follow the notation of Fig. 2. Horizontal dash-dotted line is the limit $W \to \infty$ which applies to the case in (c), only "vertical" heat sinking through the oxide. The significance of lateral 3D heat spreading from GNRs is shown in (d) and (e), both mechanisms partly leading to higher current density in the Fig. 2 inset.

To gain a physical understanding of these trends, we consider the heat spreading schematics in Figs. 3(c)–3(e). For "large" graphene in Fig. 3(c) dissipation occurs mainly "down" into the oxide. Thus, $G'' = 1/(R_{Cox} + t_{ox}/k_{ox})$ is independent of device dimensions when L, $W \to \infty$ [in practice $(LW)^{1/2} \gg 3L_H$], as shown with dash-dotted line in Figs. 3(a) and 3(b). In general, this expression may include a small heat spreading term into the Si wafer [9,17], which was negligible here [12]. For large graphene devices the constant expression is also recovered as $G'' = g/W$ when taking the limit $W \to \infty$ of Eq. (3).

In contrast, for "narrow" GNRs the lateral 3D heat spreading into the SiO_2 becomes a significant component of the overall thermal conductance of a device [Fig. 3(d)]. In addition, for "short" devices some heat is conducted along the graphene and into the contacts as well [Fig. 3(e)]. The amount of heat carried out in this manner will depend on the TC and length of the device. The three solid lines in Fig. 3(a) show what the modeled G'' predicts for $k = 50$, 250, and 500 $\mathrm{W\,m^{-1}K^{-1}}$. As the TC increases, heat is carried more efficiently along the GNR. The device length also matters for "short" GNRs with $L \leq 3L_H$, when heat generated within the graphene channel is sunk more effectively into the contacts [12,18]. As a result, the thermal conductance G'' increases as L decreases in Fig. 3(b) (also see [12]). In both cases, as the heat dissipation increases, we also see an increase in device current density as plotted in the inset of Fig. 2, thus confirming that Joule self-heating is a key current limiter in GNR devices.

Since heat dissipation is sensitive to heat flow along "short" GNRs, it is possible to extract their TC, as shown in Fig. 4. To accomplish this, we iteratively vary k within L_H in Eq. (2) until the predicted breakdown power matches the measurements, for each device (we assume a unique k for each GNR). To estimate the confidence intervals of extracted TC for our GNRs, we consider a range $R_{Cox} = 1\text{–}5 \times 10^{-8}$ $\mathrm{m^2\,K/W}$ for the graphene/SiO_2 interface thermal resistance [20–22], and an uncertainty of ± 1 layer in the GNR thickness [12]. The extracted TC along with data from the literature on "large" graphene [23–25] are displayed in Fig. 4. We find a TC range $k = 63\text{–}450$ $\mathrm{W\,m^{-1}K^{-1}}$ for our GNRs, with a median ~ 130 $\mathrm{W\,m^{-1}K^{-1}}$ (at the $T_{BD} = 600\,^{\circ}\mathrm{C}$), or ~ 80 $\mathrm{W\,m^{-1}K^{-1}}$ at 20 °C, nearly an order of magnitude lower than the TC of exfoliated graphene on SiO_2 [24]. The room temperature estimate is done by assuming a mean free path that is independent of temperature (limited by edge or defect scattering), and considering only the temperature variation of graphene heat capacity [10]. Given that we observe no clear dependence of TC on GNR size (i.e., no size effect) in Fig. 4, we surmise that here the TC is limited by edge roughness

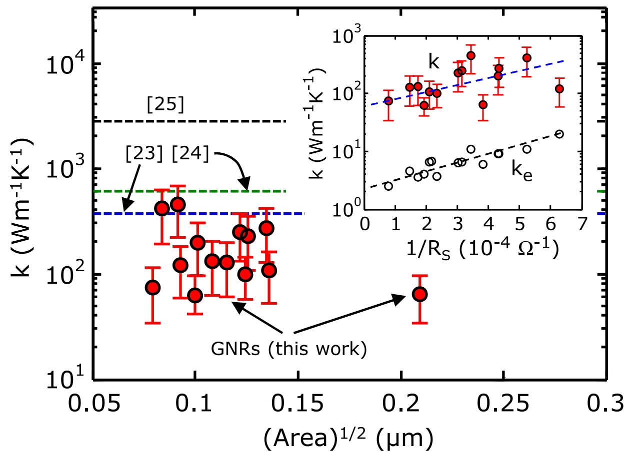

FIG. 4 (color online). Thermal conductivity (TC) of GNRs estimated in this work at T_{BD}, compared to large-area samples for supported graphene grown by CVD [23], exfoliated graphene (XG) on SiO_2 [24], and suspended XG [25]. The median TC of our GNRs at room temperature is ~80 $W m^{-1} K^{-1}$ (see text) nearly an order of magnitude lower than "large" XG on SiO_2 [24]. The inset shows approximate scaling between TC and electrical sheet conductance, suggesting scattering mechanisms common to both electrons and phonons. The electronic contribution to TC is estimated to be typically $k_e < 10$ $W m^{-1} K^{-1}$ or <10%. Dashed lines show trends to guide the eye.

and defect or impurity scattering. However, the range of values extracted can be attributed to variations in edge roughness and defect or impurity density between samples [12]. For instance, recent scanning tunneling microscopy (STM) studies [26] have found that edges of such GNRs vary from atomically smooth to ~1 nm edge roughness. Simulations [8,27] suggest that edge disorder could nearly account for the variation in TC observed in Fig. 4, while different impurity or defect density between samples will only serve to broaden the observed distribution.

To examine if the thermal and electrical properties of the GNRs are related, we plot the extracted TC vs the inverse sheet resistance ($1/R_S$) in the Fig. 4 inset. Also plotted is the electronic contribution to TC, estimated with the Wiedemann-Franz law [19] as $k_e \sim L_0 T/(R_S t)$. This estimate is likely an upper limit, as the Lorenz number in graphite is the usual $L_0 = 2.45 \times 10^{-8}$ $W \Omega K^{-2}$ [28], but in nanostructures with edge scattering it is slightly lower than this bulk value [29]. We find $k_e < 10$ $Wm^{-1} K^{-1}$, nearly always an order of magnitude lower than the extracted TC, suggesting that the TC of GNRs is dominated by phonons at room temperature and above. However, TC and electrical conductance follow similar trends, indicating that similar scattering mechanisms limit both phonon and electron transport. These scatterers include edges, impurities, and defects in GNRs [2,8,27,30].

In conclusion, we have shown that high-field transport in GNRs on SiO_2 is limited by self-heating. The maximum current density at a given temperature scales inversely with GNR width and reaches >3 mA/μm in ~15 nm wide devices. Dissipation in "large" graphene ($\gg 0.3$ μm, or 3 times the thermal healing length) is limited primarily by the SiO_2 thickness, but dissipation in "small" GNRs improves from 3D heat spreading into the SiO_2 and heat flow along the GNR to the contacts. Taking advantage of this sensitivity we found a median TC ~80 $W m^{-1} K^{-1}$ for GNRs at room temperature, with less than 10% electronic contribution.

We acknowledge funding from the Marco MSD Center, the ONR MURI, AFOSR YIP, and the NRI.

*hdai@stanford.edu
†epop@illinois.edu

[1] A. Cresti et al., Nano Res. **1**, 361 (2008).
[2] X. Wang et al., Phys. Rev. Lett. **100**, 206803 (2008).
[3] M. Lazzeri and F. Mauri, Phys. Rev. B **73**, 165419 (2006).
[4] E. Pop et al., J. Appl. Phys. **101**, 093710 (2007).
[5] A. Javey et al., Phys. Rev. Lett. **92**, 106804 (2004).
[6] Y. F. Chen and M. S. Fuhrer, Phys. Rev. Lett. **95**, 236803 (2005).
[7] A. Liao, Y. Zhao, and E. Pop, Phys. Rev. Lett. **101**, 256804 (2008).
[8] W. Li et al., Phys. Rev. B **82**, 041410 (2010).
[9] E. Pop, Nano Res. **3**, 147 (2010).
[10] A. Liao et al., Phys. Rev. B **82**, 205406 (2010).
[11] L. Jiao et al., Nature Nanotech. **5**, 321 (2010).
[12] See supplemental material at http://link.aps.org/supplemental/10.1103/PhysRevLett.106.256801 for sample fabrication, contact resistance, spreading thermal resistance, and model details.
[13] H. Y. Chiu et al., Phys. Rev. Lett. **95**, 226101 (2005).
[14] A. M. Katzenmeyer et al., IEEE Trans. Nanotechnol. **10**, 92 (2011).
[15] A. I. Savvatimskiy, Carbon **43**, 1115 (2005).
[16] M.-H. Bae et al., Nano Lett. **10**, 4787 (2010).
[17] V. E. Dorgan, M.-H. Bae, and E. Pop, Appl. Phys. Lett. **97**, 082112 (2010).
[18] E. Pop, Nanotechnology **19**, 295202 (2008).
[19] C. Kittel, *Introduction to Solid State Physics* (John Wiley & Sons, Hoboken, NJ, 2005).
[20] Z. Chen et al., Appl. Phys. Lett. **95**, 161910 (2009).
[21] K. F. Mak, C. H. Lui, and T. F. Heinz, Appl. Phys. Lett. **97**, 221904 (2010).
[22] Y. K. Koh et al., Nano Lett. **10**, 4363 (2010).
[23] W. Cai et al., Nano Lett. **10**, 1645 (2010).
[24] J. H. Seol et al., Science **328**, 213 (2010).
[25] S. Ghosh et al., Nature Mater. **9**, 555 (2010).
[26] C. Tao et al., Nature Phys., doi:10.1038/nphys1991 (2011).
[27] A. V. Savin, Y. S. Kivshar, and B. Hu, Phys. Rev. B **82**, 195422 (2010).
[28] M. G. Holland, C. A. Klein, and W. D. Straub, J. Phys. Chem. Solids **27**, 903 (1966).
[29] F. Völklein et al., Nanotechnology **20**, 325706 (2009).
[30] T. Fang et al., Phys. Rev. B **78**, 205403 (2008).